Journal of
Mechanical
Science and
Technology

Journal of Mechanical Science and Technology 21 (2007) 1828~1846

False diffusion in numerical simulation of combustion processes in tangential-fired furnace

Xuchang Xu*, Zhigang Wang, Yuqun Zhuo and Changhao Zheng

Thermal Engineering Department Tsinghua University, Beijing 100084, China

(Manuscript Received May 7, 2007; Revised August 6, 2007; Accepted August 7, 2007)

Abstract

Numerical simulation serves as one of the most important tools for analyzing coal combustion in Tangentially Fired Furnaces (TFF) with NUMERICAL FALSE DIFFUSION as one key problem that degrades the simulation accuracy, especially for complex flow patterns. False diffusion often completely compromises the accuracy, leading to erroneous predictions. This paper reviews various methods to reduce the numerical diffusion. In computational fluid dynamics (CFD), false diffusion originates from a truncation error of the Taylor series approximation of the derivative and multi-dimensional discretization effects. Higher-order upwind convective schemes were designed to reduce truncation errors, while grid line adjusting methods were developed to reduce crossflow diffusion. This paper compares numerical and experimental results for isothermal flows to evaluate these methods. Results with the standard upwind scheme in a rectangular Cartesian mesh are compared with results in body-fitted meshes for comprehensive combustion processes in a TFF. Analysis of the false diffusion effect in the x, y, z directions and the artificial viscosity distribution in a rectangular mesh shows where the false diffusion overtakes the real physical diffusion and where the mesh must be refined or grid line must be adjusted to improve TFF combustion simulations.

Keywords: Numerical false diffusion; Convection diffusion; Tangentially Fired Furnace (TFF); Truncation error; Crossflow diffusion

1. Introduction

Tangentially fired furnaces (TFF) in utility boilers, sometimes called corner-fired furnaces, are frequently used in combustion systems for gas, oil, bituminous and sub-bituminous coal and lignite for electricity generation. Nowadays, tangentially fired furnaces are also widely used to burn anthracite and low-volatile coals in China. Empirical methods are used to analyze equipment performance and for furnace development while CFD (Computational Fluid Dynamics) codes incorporating models for turbulent flow, radiation, and chemical reactions are also powerful tools. "Empirical development is still necessary, but this is greatly aided by the insights gained from CFD studies, not only of the particular devices of practical interest, but also of the simpler model problems that have been studied in detail by combustion scientists" [1]. However, better numerical methods are needed for these furnaces for boiler retrofits, operation optimization [2], temperature distribution prediction [3] and for predicting performance when operating parameters, physical and chemical conditions in the TFF are changed [4].

The quasi-symmetric combined injections from the burners in the TFF form a weakly swirling flow. After the combustion section, near the furnace exit, the flow eventually develops into a weakly symmetric swirling flow in a tower type furnace, or an asymmetric nearly non-swirling flow in a Π type furnace. Simple convection treatment with simple mesh arrangements such as rectangular meshes near the burners will result in false diffusion and unreasonable results.

False diffusion is a major problem in convection-diffusion fluid flow simulations, which causes con-

*Corresponding author. Tel.: +86 10 6277 3153, Fax.: +86 10 6277 0209
E-mail address: xxc-dte@mail.tsinghua.edu.cn

siderable numerical errors in numerical analyses. First order schemes, such as the upwind, power law and hybrid schemes, give stable computational convergence, but they introduce false diffusion which compromises numerical accuracy [5]. False diffusion has generated much confusion but can be controlled by computational skills. This review gives a brief analysis of false diffusion with advice on how to reduce false diffusion in TFF combustion simulations. Different ways to reduce false diffusion in TFF flow field simulations are also illustrated with experimental validation. The false diffusion effects in comprehensive combustion simulations are illustrated by comparing results of the upwind scheme with a rectangular mesh and the upwind scheme with a body-fitted mesh. The false diffusion effects and artificial viscosity in a rectangular mesh in a TFF are calculated to show the effects.

Inaccurate flow field predictions will affect the other scalar convection-diffusion processes so that combustion simulations will be inaccurate. Therefore, fluid dynamics simulations with less false diffusion will provide better simulations of the combustion processes in the TFF.

The simulated velocity fields at pulverized coal combustion processes on a cross section in the TFF at a height of 1600 cm in the utility boiler HG-670/140-9 predicted using the body-fitted and rectangular meshes are compared in Fig. 1. The injected flow in the rectangular mesh is quickly attenuated because of the strong crossflow diffusion effects introduced by the first order upwind scheme so that the injected flows from the burner incorrectly reach the water wall very quickly. In the body-fitted mesh with less false diffusion effect, the injected flows reach further outinto the center of the furnace to form a swirling counter-clockwise rotation. At the same time the calculated combustion processes of fuel particles, gas temperature and composition distributions are very different by using these two mesh systems. This will be discussed in detail later in this paper.

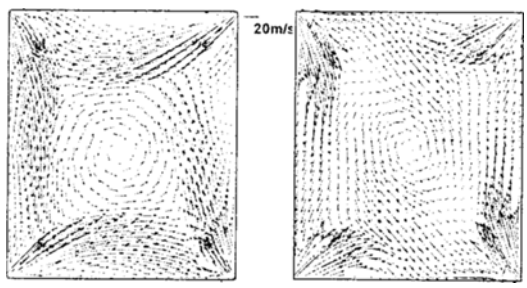

Body-fit mesh Rectangular mesh

Fig. 1. Velocities for combustion in TFF at a height of 1600 cm of boiler HG-670/140-9.

2. Origin of false diffusion

Combustion processes are usually modeled by equations including convection and diffusion terms (1). However, these differential equations cannot be solved to obtain exact solutions; hence, they must be solved numerically by discretizing the convection and diffusion terms.

The general convection-diffusion equation is:

$$\frac{\partial(\rho\phi)}{\partial t} + div(\rho\vec{V}\phi) = div(\Gamma grad\phi) + S \tag{1}$$

The four terms in the generalized differential equation are the transient term, advective term, diffusion term and source term, respectively. The diffusion coefficient Γ, and the source term S, depend on the variable of interest denoted by ϕ. The diffusion term in Eq. (1) is usually discretized by using central differences with second-order accuracy, which is accurate enough for most problems in practice [6]. Difficulties arise with the advective term in Eq. (1). Central differencing can lead to un-physical oscillatory behavior in an implicit solution or to disastrous divergence in an explicit computation in regions where convection strongly dominates diffusion [7] and first order methods which aim to avoid computational oscillations are used leading to the well-known false diffusion effect in computational fluid dynamics (CFD). First-order upstream differencing often suffers from severe inaccuracies due to truncation errors and streamline-to-grid skewness [8]. In general, false diffusion originates from truncation error which can be written as:

$$E_s'(\eta) = \left[\sin(2\theta)(\cos\theta+\sin\theta)\right](\alpha-\beta)U(\Delta\xi)\frac{\partial\phi}{\partial\eta} + \left[\frac{\sin(2\theta)}{2}\left(\cos^2\theta-\sin^2\theta\right)\right]\left(\beta-\gamma-\frac{1}{6}\right)U(\Delta\xi)^2\frac{\partial^2\phi}{\partial\eta^2}+\ldots \tag{2}$$

In which $E'(\eta)$ is the truncation error, ϕ is the scalar of interest; α, β and γ are associated with advective schemes; θ is the angle between velocity and grid line;

η is the direction normal to the streamline; $\Delta\xi$ is grid interval.

It is clear from Eq. (2) that there are three ways to reduce false diffusion: corrective advective schemes, grid line adjustment and grid refinement. False diffusion effect is also combined with the scalar gradient in the direction normal to the streamline which is beyond the control of numerical skills.

3. Evaluation of false diffusion

A numerical model with false diffusion would be given by [9]:

$$\rho\left(u\frac{\partial\phi}{\partial x}+v\frac{\partial\phi}{\partial y}\right)= (\Gamma+\Gamma'_x)\frac{\partial^2\phi}{\partial x^2}+(\Gamma+\Gamma_y')\frac{\partial^2\phi}{\partial y^2} \tag{3}$$

where Γ'_x and Γ'_y are false diffusion coefficients introduced by the first-order upwind scheme. In a coordinate system with the axis aligned with the local flow direction, the discretized model is approximately [9]:

$$\rho|V|\frac{\partial\phi}{\partial s}=\Gamma\left(\frac{\partial^2\phi}{\partial s^2}+\frac{\partial^2\phi}{\partial n^2}\right)+ \Gamma'_s\frac{\partial^2\phi}{\partial s^2}+\Gamma'_{sn}\frac{\partial^2\phi}{\partial s\partial n}+\Gamma'_n\frac{\partial^2\phi}{\partial n^2} \tag{4}$$

In which

$$\Gamma'_s=0.5|V|(\Delta x\cos^3\theta+\Delta y\sin^3\theta) \tag{5}$$

$$\Gamma'_{sn}=0.5|V|(\Delta y\sin\theta-\Delta x\cos\theta)\sin 2\theta \tag{6}$$

$$\Gamma'_n=0.5|V|(\Delta x\cos\theta\sin^2\theta+\Delta y\sin\theta\cos^2\theta) \tag{7}$$

where θ is the angle between the velocity and the x-axis. The last three terms result from the false diffusion in the multi-dimensional space. Γ'_s is the streamwise diffusion coefficient, Γ'_n is the cross-flow diffusion coefficient normal to the flow and Γ'_{sn} is the combined diffusive effects in the streamwise and normal directions. For most flows, $\frac{\partial^2\phi}{\partial n\partial s}$ is not significant; thus the product of Γ'_{sn} and $\frac{\partial^2\phi}{\partial s\partial n}$ can be neglected. For $\Delta x = \Delta y$, the cross diffusion coefficient Γ'_n is maximized at $\theta = 45°$, but is zero if the flow is aligned with either the x or y directions. In contrast, the streamwise diffusion coefficient Γ'_s maximized at $\theta = 0°$ or 90° and minimized at θ=45°. In Fig. 2, the vertical axis corresponds to $\Gamma'/(0.5|V|\Delta)$, where $\Delta = \Delta x = \Delta y$. The streamwise diffusion coefficient seems to be of more concern since for $\Delta x = \Delta y$, $|\Gamma'_s| \geq |\Gamma'_n|$ for $0 \leq \theta \leq 90°$. However, for most engineering flows with scalars transported by the flows, the streamwise gradient can be neglected ($\partial^2\phi/\partial n^2 >> \partial^2\phi/\partial s^2$) so the cross-flow diffusion introduces more significant errors than the streamwise diffusion if the local flow direction does not coincide with the grid lines.

For the engineering applications given in this paper, the false diffusion will concentrate mainly on cross-flow numerical diffusion, which has a much larger effect on the accuracy of the results than the streamwise diffusion.

The false diffusion coefficients were investigated by Kang et al. [10] for two-dimensional flows with the conclusions extended to three-dimensional flows. In a three-dimensional flow, the false diffusion coefficients are given by:

$$\begin{cases}\Gamma_{cfx}=u\Delta x(1-p_x)\\ \Gamma_{cfy}=v\Delta y(1-p_y)\\ \Gamma_{cfy}=w\Delta z(1-p_z)\end{cases} \tag{8}$$

where

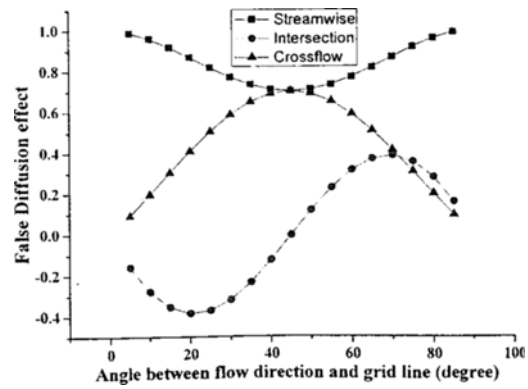

Fig. 2. Streamwise, crossflow diffusion and interaction diffusion.

$$\begin{cases} p_x = (u/\Delta x)/(u/\Delta x + v/\Delta y + w/\Delta z) \\ p_y = (v/\Delta y)/(u/\Delta x + v/\Delta y + w/\Delta z) \\ p_z = (w/\Delta z)/(u/\Delta x + v/\Delta y + w/\Delta z) \end{cases} \quad (9)$$

Eqs. (8-9) give the false diffusion effect in three directions which can be used to evaluation difference between the numerical effect and physical diffusion effect in the flow simulation.

4. False diffusion reduction methods

4.1 Convective term discretization

False diffusion originates from truncation error which is associated with convective scheme [Eq. (2)], and it is produced by single-side lower order upwind schemes. Higher-order upwind schemes were developed to achieve more numerical accuracy. QUICK (Quadratic Upstream Interpolation for Convection Kinematics) [11], Second-order Upwind [12], COPLA [13], EULER [14], HLPA(Hybrid linear parabolic approximation) [15], MINMOD (Minimum modulus) [16], MUSCL (Monotonic upwind scheme for conservation law) [17], OSHER [18], skew up-wind [19] and 27-point scheme [20] are high-order upwind wise schemes which can reduce truncation error and maintain numerical stability. Mathematic description of these methods will not be repeated in detail in this paper. We used two classic high-order upwind schemes: QUICK and SUD, to evaluate the false diffusion reduction effect of convective schemes.

4.2 Mesh improvements

Grid refinement and grid line adjustment can also reduce false diffusion effect in numerical simulation. Grid generation for grid line adjustment will be described in detail in this section. After mesh improvements introduction we used these meshes to simulate flow field in a scaled furnace [21] and numerical results will be validated with experiment data.

A rectangular mesh, a refined rectangular mesh, a body-fitted mesh and an O type mesh (Fig. 3) have been used to simulate the flow in a scaled furnace of a 670 t/h steam boiler [22, 23]

Air injected into the furnace from the corner burners formed a weakly swirling up flow which becomes a non-swirling flow with several parallel branches divided by the steam superheater screens in the upper region in the furnace as shown in Fig. 4. In the top section of the TFF, the rectangular mesh has grid lines aligned with the flow direction due to the convenient mesh generation near the steam superheater screens hanging from the top of the furnace. Interface interpolation was used to interpolate between the rectangular mesh in the upper or lower regions in the scaled TFF and the three meshes (Fig. 3) used in the combustor section.

The rectangular mesh used a total of 383,744 cells for the scaled TFF. The refined rectangular mesh used a large number of cells in the combustor section with a total of 1,634,344 cells.

The grid lines in the body-fitted mesh were oriented nearly to the velocity direction in the horizontal plane. The TFF body-fitted mesh was generated by numerical solutions of elliptic partial differential Poisson equations with specified control functions for the node locations done in the transformed coordinate system. The corresponding transformed equation can be written in vector form as:

$$g^{ij}\frac{\partial^2 \boldsymbol{r}}{\partial \xi^i \partial \xi^j} + (g^{kk} p^k)\frac{\partial \boldsymbol{r}}{\partial \xi^k} = 0 \quad (10)$$

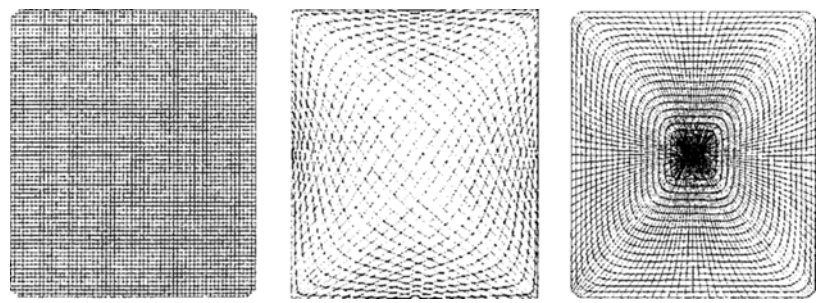

(a) Rectangular mesh (b) Body-fitted Mesh (c) O type Mesh

Fig. 3. Mesh topologies [21].

where $r = x_m i_m$.

The control function, p^k, was the exponential function:

$$\begin{cases} p^k = -\sum_{l=1}^{n} a_l \mathrm{Sgn}(\xi^k - \xi^l)\exp(-b_l T_l) \\ T_l = \sqrt{\sum_{l=1}^{n} C_{lk}(\xi^k - \xi^l)^2} \end{cases} \quad (11)$$

The procedure specifies the boundary nodes which were then transformed from the computational domain to the physical domain. Due to the complexity of the mesh configuration, the procedure cannot be completed directly. As shown in Fig. 5b, Mesh B, the uniform mesh in the computational domain in the first step of mesh B is transformed into the new domain so that it intersects the four corners of the original physical boundary. The boundary nodes can be more easily specified in this simple configuration in the transformed domain than in the physical domain. Then the boundary nodes in the transformed domain are projected back into the physical boundaries. Finally, the transformed mesh is projected back into the physical domain. The furnace model then had a final total of 51,300 elements.

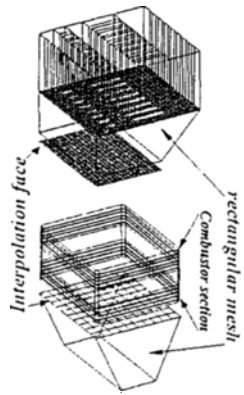

Fig. 4. Mesh arrangements in the different topologies.

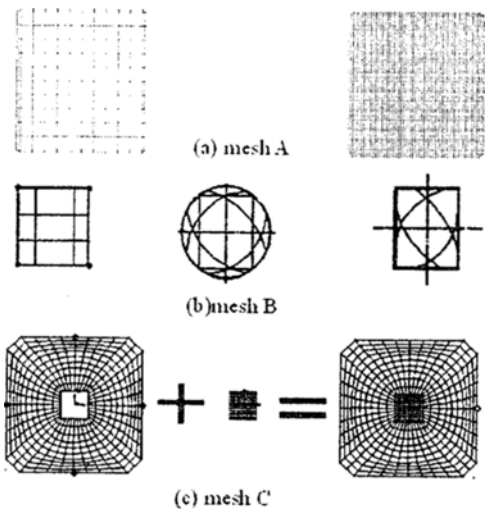

Fig. 5. Mesh topology generation.

The O type mesh shown in Fig. 3c is used when the interior boundaries are important [22]. The grid lines in the central area are fit to a small central rectangle. The main disadvantage of this mesh is the large number of elements in the center region with as many elements as in the rest of the horizontal mesh. This large number of elements is not necessary in the center region which has no sharp gradients of the physical variables. This mesh had a total of 217,240 elements.

5. The coal combustion simulations and diffusion effects in utility boilers

Combustion is one of the most difficult processes to model mathematically since it involves the simultaneous processes of three-dimensional, multi-phase fluid dynamics, turbulent mixing, fuel evaporation, radiative and convective heat transfer, and chemical reactions. In the past twenty years, comprehensive combustion simulation codes [24-30] and commercial software packages [31-33] have been employed to investigate combustion processes in utility boilers. Models have been developed for turbulent flows, two-phase flows, heterogeneous two-phase reactions, radiation [34] and ash deposition [35].

Smoot et al. [27, 29] developed a combustion code with the name "PCGC-3" which used the EBU model for the turbulent combustion and the DO method to predict the radiative heat transfer. They used a staggered rectangular mesh with 52×52×84=227,136 elements. Comparison of the predicted particle behavior [36, 37] and local temperatures [38] in this industrial-scale pulverized tangentially-fired furnace (TFF) from PCGC-3 and Fluent with experimental data for an 85 MWe pulverized coal boiler (tangentially-fired furnace) showed that the simulation captures the qualitative trends observed in the furnace except in the burner and near-wall regions.

Simulations of tangentially fired combustion [39-42] have included comprehensive coal combustion models well coupled to the rest of the analysis with the simulation results agreeing with experimental data. Furnace operating conditions and parameters of combustion models have been investigated numerically with rectangular meshes widely used in these simulations. "The nature of comprehensive combustion models is such that they require use in their present state of development by a technical specialist with appropriate training, back-ground and experience and much work remains to be done" [28]. In the early years, the importance of false diffusion was not well recognized and rectangular mesh with lower-order convective schemes was widely used to simulate tangentially fired combustion. In recent years, the false diffusion effect has been addressed with the rapid developments of computational techniques and computer hardware [43-46]. Higher-order convective schemes [47-50], mesh adjusting methods [51-55] and artificial viscosity methods [56-58] have been developed to prevent the false diffusion caused by convective schemes and rectangular meshes in TFF combustion simulations. The artificial viscosity method requires correct prediction of the false diffusion distribution across the computational domain with negative viscosities used in the discretized equations to eliminate the false diffusion. This method adds complexity and computational expense as seen in the following equations [56]:

$$\nabla\cdot[V\cdot\nabla V]=\nabla\cdot[\Gamma_{\text{artificial}}T\cdot\nabla V] \tag{12}$$

$$T=\begin{pmatrix}\cos^2 A & \cos A\cos B & \cos A\cos C\\ \cos A\cos B & \cos^2 B & \cos B\cos C\\ \cos A\cos C & \cos B\cos C & \cos^2 C\end{pmatrix} \tag{13}$$

$$\Gamma_{\text{artificial}}=\left[\text{cth}\left(\frac{R_{e\Delta}}{2}\right)-\frac{2}{R_{e\Delta}}\right]\frac{|V|\Delta}{2} \tag{14}$$

$$\Delta=\frac{1}{3}(\Delta x+\Delta y+\Delta z) \tag{15}$$

$$R_{e\Delta}=\frac{|V|\Delta}{(v+\Gamma_{\text{artificial}})} \tag{16}$$

The following section will compare several of these advection discretization schemes and mesh arrangements with experimental data.

6. Comparison of various simulation schemes for tagentially fired furnaces

6.1 Phase doppler particle anemometer (PDA) measurement

6.1.1 Model system and boundary conditions

The flow field was measured in an HG-670/140-9 TFF boiler under room temperature [54]. The total height of the furnace model was 2200 mm and the cross section was 580 mm×680 mm. Each corner had two groups of combustors as shown in Fig. 6. The primary, secondary and auxiliary air streams were allocated separately with a primary air velocity of 17 m/s, a secondary air velocity of 25 m/s and an auxiliary air velocity of 30 m/s based on the physical model with velocity components as listed in Table 1.

6.1.2 Measurement locations and PDA system

The scale model furnace was constructed with glass windows as shown in Fig. 7 with a superheater made of 4 mm aluminum alloy planes to avoid static electricity and vibrations. The furnace outlet had a convergent duct and cyclone. The air flow was controlled by valves for each air inlet and measured by Venturi meters. The glass particles passed through a flexible tube from the hopper to each air inlet.

A 3D-PDA system with a 58N50 Enhanced Signal Processor [59] from DANTEC(1994) was used to measure the flow velocities. The velocities were measured at three horizontal sections. Each section had 18 measurement points. Data were not obtained near the wall due to difficulties in manipulating the probe through the sampling windows.

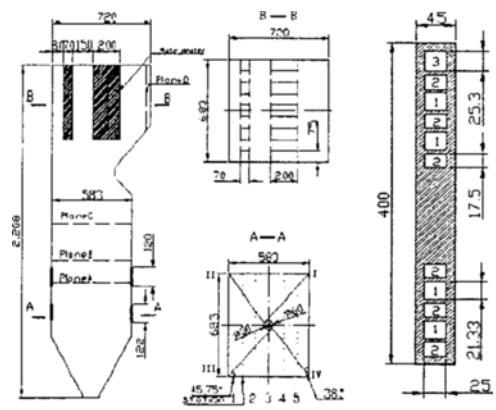

Fig. 6. (a) Schematic of 670 t/h furnace model structure [60], (b) Burner mouth model size.

The unweighted velocities were averaged by simple averaging residence time weighting and interval time weighting.

$$\vec{U} = \frac{\sum U_i \Delta t_i}{\sum \Delta t_i} \tag{17}$$

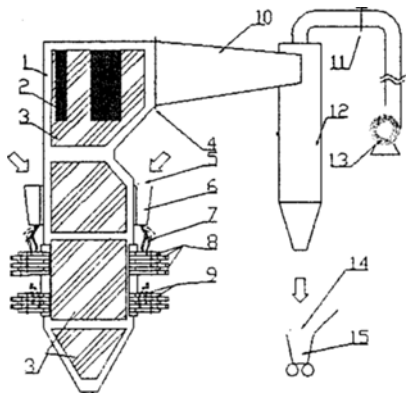

Fig. 7. Furnace schematic for 3D-PDA measurement 1. furnace, 2. superheater, 3. glass windows, 4. perforated plate, 5,14. tracking glass particles, 6. powder storage, 7. flexible tube, 8. air inlet, 9. Venturi nozzle and valve, 10. Convergent duct, 11. Seal Valves, 12. cyclone separator, 13. air blower, 15. recycling tank.

Table 1. Boundary conditions in the furnace model [60].

	Size (mm^2)	(m/s)	Position (Fig.6a :A-A)			
			Corner I	II	III	IV
Primary air	21×25	u	-12.02	10.71	12.02	-0.71
		v	-12.3	-13.46	12.03	13.46
Secondary air	17.5×25	u	-17.37	15.48	17.37	15.48
		v	-17.78	-19.46	17.78	19.46
Auxiliary air	25×25	u	-25.07	22.34	25.07	22.34
		v	-25.67	-28.08	25.67	28.08

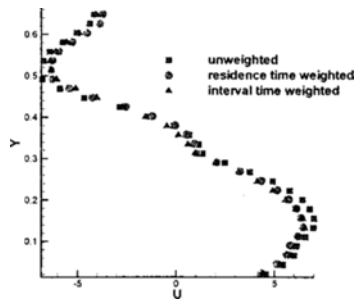

Fig. 8. Comparison in calculating velocity by using different statistical methods at the central position inside furnace [60].

Fig. 8 shows that the averaging methods produced different results in the high velocity regions with the residence time weighted and interval time weighted velocities being similar.

6.2 Numerical modeling and results validation

6.2.1 Curvilinear coordinate system

The continuity equation can be expressed in terms of primitive variables as:

$$\frac{\partial}{\partial \xi^i}\left(\frac{\rho V^i}{J}\right) = 0 \tag{18}$$

where J is the Jacobian of the transformation:

$$\frac{1}{J} = \frac{\partial(x,y,z)}{\partial(\xi^1,\xi^2,\xi^3)} \tag{19}$$

The strong conservative form [61] of the momentum equation in a general curvature coordinate system can be written in terms of the primitive variables as:

$$\frac{\partial}{\partial \xi^i}\left(\frac{\rho V^i}{J} u_j\right) = \frac{\partial}{\partial \xi^i}\left(\mu \frac{g^i \cdot g^k}{J} \frac{\partial u_j}{\partial \xi^k}\right) - I \frac{g}{J} \frac{\partial p}{\partial \xi^i} \tag{20}$$

where $V_i = g_i \cdot V$ is contravariant velocity component in the curvilinear coordinate system and u_j is the velocity component in the fixed Cartesian coordinate system.

Four meshes were generated for the numerical analysis of the fluid dynamics in a TFF at room temperature for comparison with the experimental data.

The standard k-ε model was employed to simulate the turbulence with the same standard k-ε parameters used for all four meshes. The inlet turbulence intensity was 10% with the characteristic length equal to the hydraulic diameter of the air inlets (Primary air: 2.1 cm, Secondary air: 1.7 cm, Auxiliary air: 2.5 cm).

Six cases were chosen for the isothermal flow fluid simulations. Case A used a rectangular mesh with the upwind scheme, case B used a body-fitted mesh with the upwind scheme, case C used an O-type mesh with the upwind scheme, case D used a refined rectangular mesh with the upwind scheme, case E used the same rectangular mesh as case A with the QUICK scheme, and case F used the same rectangular mesh as case A with the second-order upwind (SUD). The conver-

gence criteria are listed in Table 2.

6.2.2 Results validation

Case A (rectangular mesh) was the simplest treatment among these six cases with a rectangular mesh and the first-order upwind scheme to simulate the tangential isothermal flow field. As a result, case A had the fastest convergence. Any grid refinements or improved convective schemes will increase the computational time.

The false diffusion effects were evaluated by comparing the u-v vectors and the w distribution. Reduction of the false diffusion effects will increase the injection jet velocities near the burner mouth. These air velocities are an important factor in the result evaluations.

Fig. 9(a) shows that the improved mesh arrangement and the improved upwind schemes both enhanced these air injection velocities. The results for the body-fitted mesh and the O type mesh most effectively predicted the injection jet velocities.

Experimental measurements [60, 62] in a TFF showed that the w velocity distribution changed from a "W" to an "M" shape in the central vertical section inside the furnace as shown on the left side figure of Fig. 10. At the burner mouth level, the w velocities in the center were positive while the velocities near the two sides were negative in the experiments. Above the burner level, the w distribution reversed with the w velocities in the center being negative and gradually becoming less negative towards the outside. These w velocity distributions are the two main characteristics of the TFF isothermal flow at room temperature. W velocity is much smaller compared to the U and V velocities and is difficult to measure precisely, but the transformation of "w" to "m" of W velocity is clear in tangentially fired furnaces. As a matter of fact, O type and body-fitted meshes have some advantages over square and refined square meshes. The results for cases D, E and F are similar to those for case A while the calculated results for cases B and C are close to the experimental results.

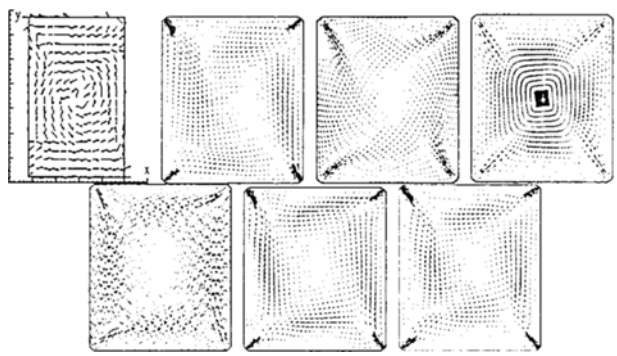

(a) u-v vectors

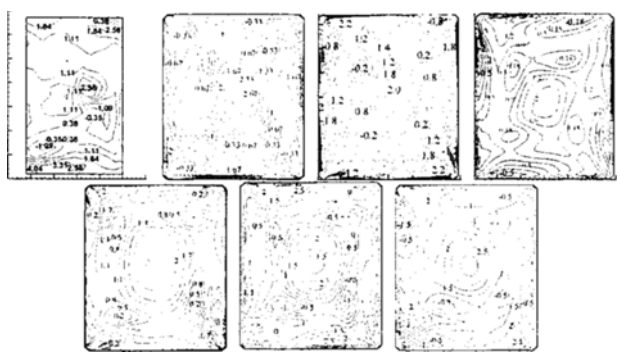

(b) w contour

Experiment [60] A: Rectangular B: Body-fitted C: O-type D: Refined rectangular mesh E: Rectangular mesh with QUICK F: Rectangular mesh with SUD

Fig. 9. u, v vectors and w contours of Plane B, respectively.

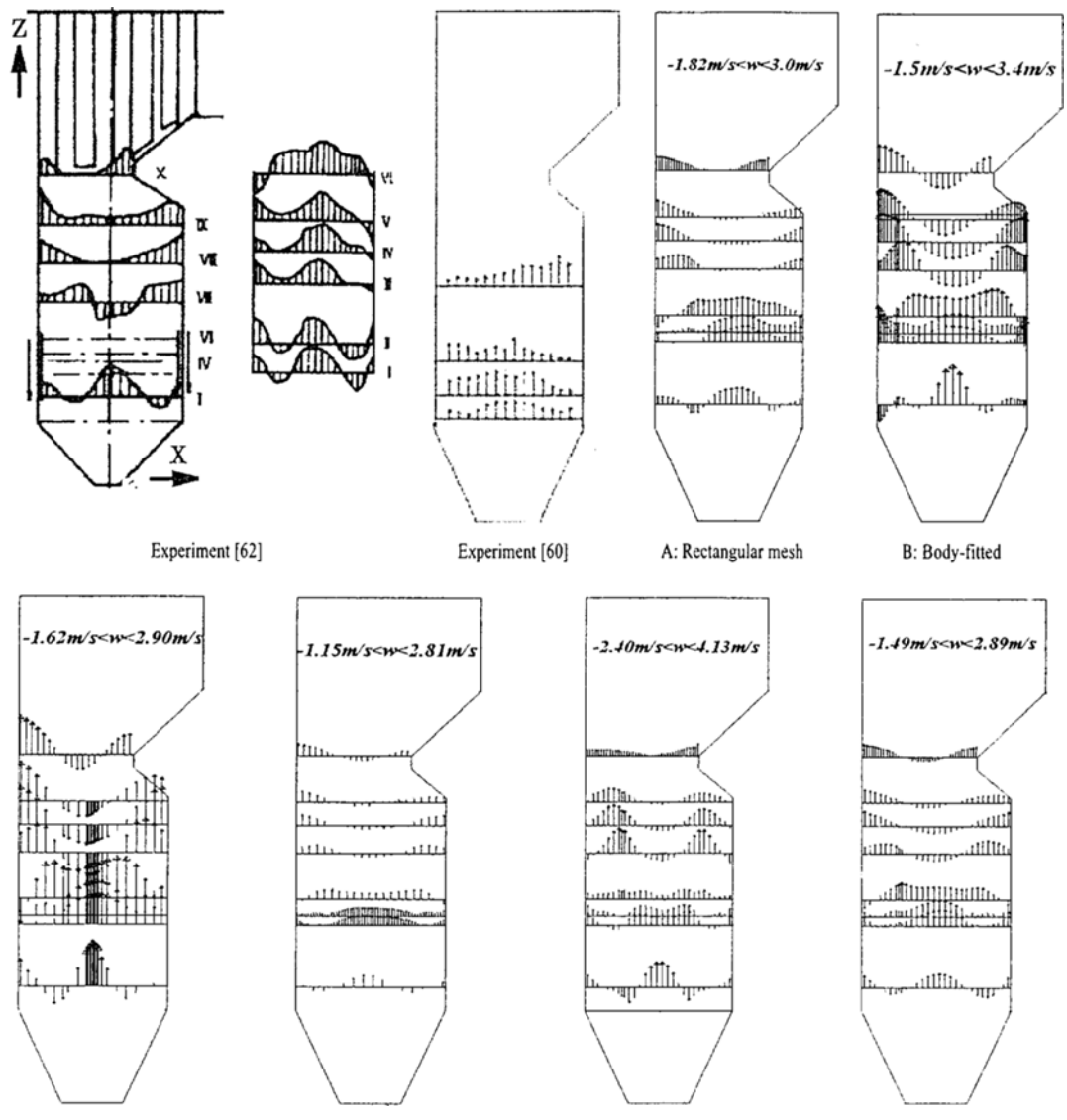

Fig. 10. Z-direction velocity contour comparison in different meshes with experiments.

Table 2. Convergence criteria and computational times.

Computation Scheme	Mass balance $\% \times 10^{-05}$	u% $\times 10^{-6}$	v% $\times 10^{-3}$	w% $\times 10^{-4}$	k% $\times 10^{-3}$	ε% $\times 10^{-5}$	Steps until Conver-gence	Time per step (s)
A: Rectangular mesh	0.015	4.44	0.981	9.9903	0.318	0.021	1822	8.0
B: Body-fitted	-0.499	3.59	0.995	5.35	0.246	0.0372	3324	3.4
C: O-type	1.37	2.93	0.999	4.86	0.230	0.0396	1981	4.6
D: Refined rectangular mesh	-0.039	2.337	0.668	9.977	0.653	0.042	1824	44.3
E: QUICK with rectangular mesh	-0.008	3.31	0.481	8.18	0.424	0.114	3804	8.2
F: SUD with rectangular mesh	0.003	0.225	0.110	0.975	0.064	1.08	3914	8.2

Detail experimental validations are necessary to evaluate the simulation results. The v and w velocities at the three horizontal measurement sections are compared with the experimental data in Figs. 11(a)

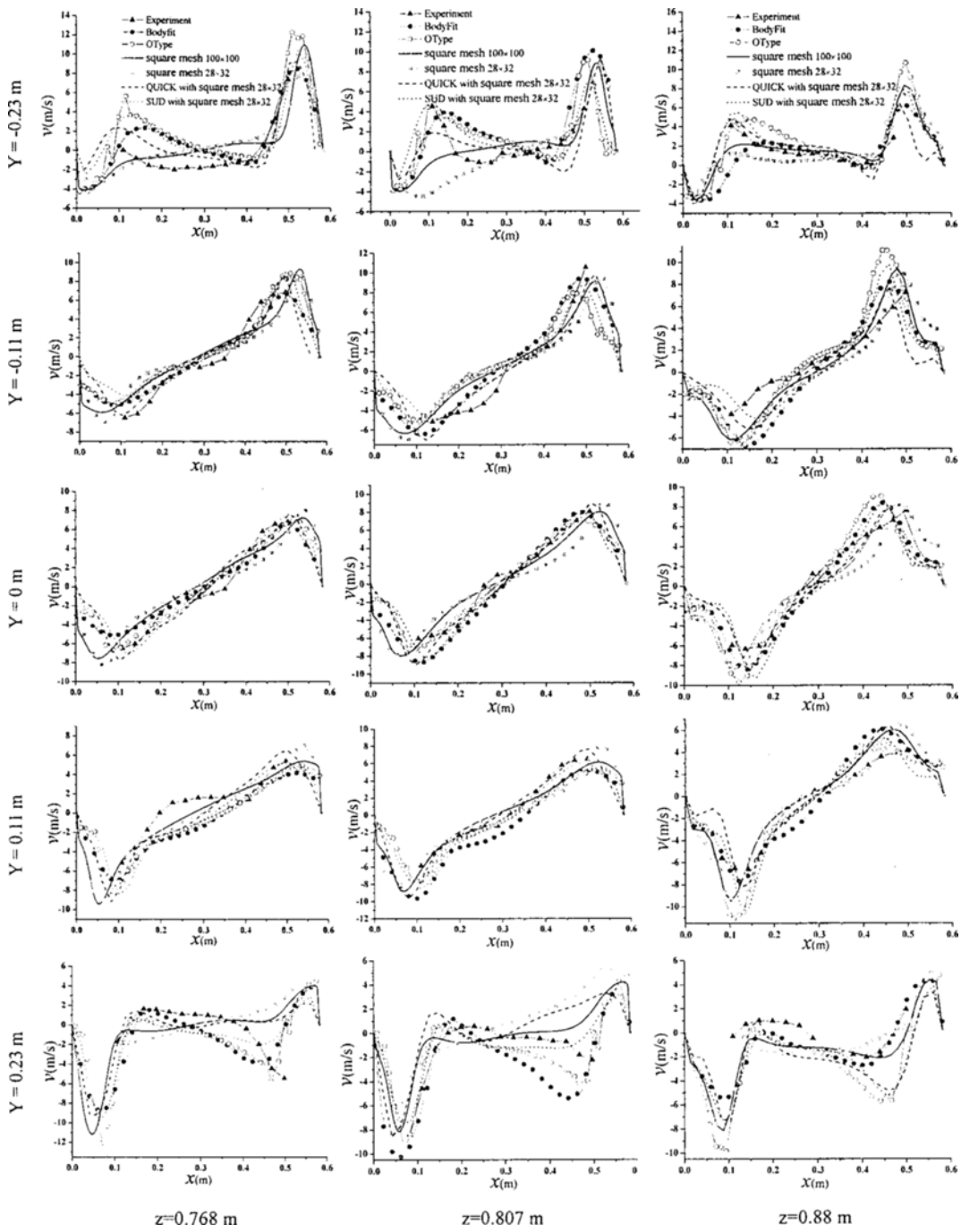

Fig. 11(a). Different mesh computational v velocity comparison with PDPA experiment.

and 11(b).

The results in Fig. 11(a) show that the predictions of the body-fitted and O type meshes are close to each other and to the experimental data and that the predictions using the rectangular mesh are improved by the mesh refinements and the higher order upwind schemes.

The simulation results in Fig. 11(b) show that the central w velocity distribution changes from a "W" to an "M" shape, which is very typical of the isothermal

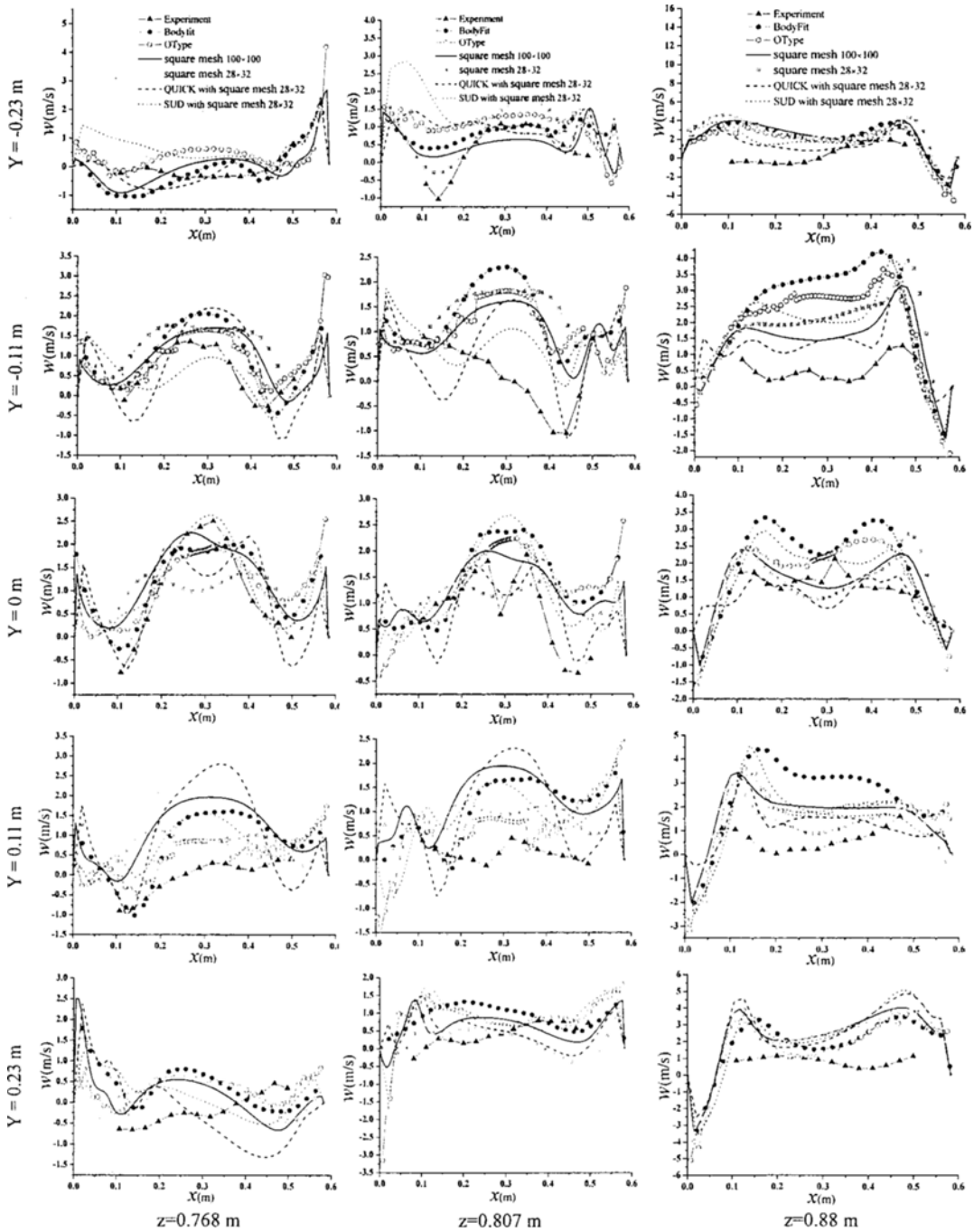

Fig. 11(b). Different mesh computational w velocity comparison with PDA experiment.

w velocity distribution inside the TFF, seen in Fig. 11(b) y=0 m row.

6.3 False diffusion magnitude

The false diffusion coefficients Eqs. 8 and 14 in the rectangular TFF mesh were evaluated to assess the magnitudes of the various effects to evaluate the crossflow diffusion in the TFF fluid dynamic simulations.

The crossflow diffusion coefficients for the rectangular TFF mesh and the artificial viscosity distributions are illustrated in Figs. 12(a) and 12(b).

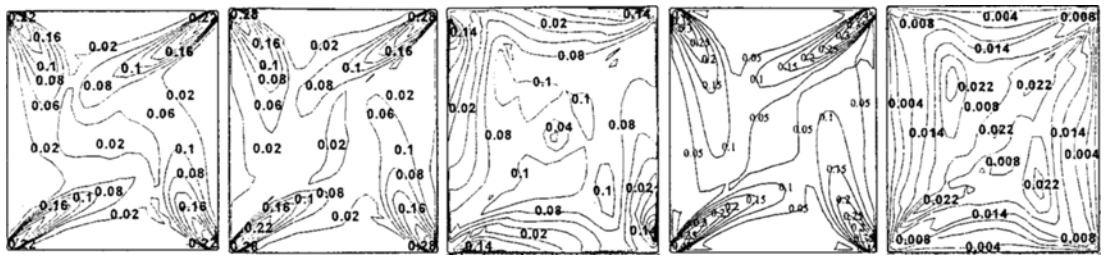

Fig. 12(a). False diffusion and viscosity distribution at rectangular mesh in horizontal section.

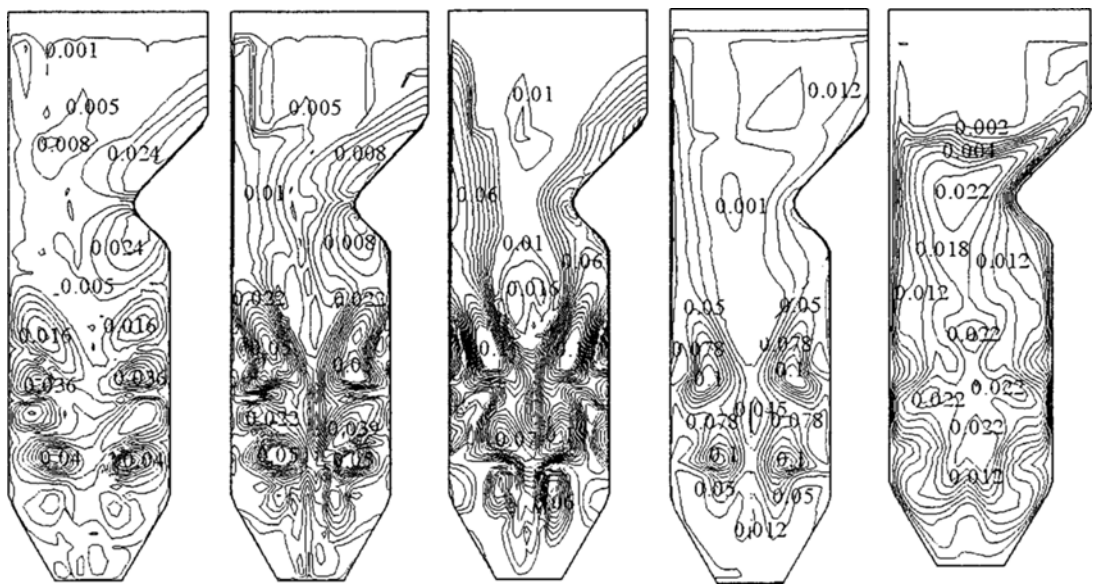

Fig. 12(b). False diffusion and viscosity distribution of rectangular mesh in vertical section

The data in Fig. 12(a) was calculated on plane A at the burner level in the model furnace shown in Fig. 6 which was at a height of 0.85 m in the air injection zone.

The numerical results show that the x-direction and y-direction crossflow numerical diffusion near the injectors is much higher than in the interior which agrees with Davis and Mallinson's approximation and Kang's result [10]. Near the four corners, the angle between the velocity vectors and the axis was about 45°, which gives the maximum false diffusion, and the artificial viscosity due to the numerical diffusion is 10~30 times higher than the turbulent viscosity near the injectors where the turbulent viscosity is relatively low. Hence, in the inlet area, strong false diffusion effects in the convection-diffusion equation lead to unrealistic flow predictions. If false diffusion was reduced by grid refinements, the number of grid cells will be over ten times of original grid cells in one direction and in three directions, total cells will be over one thousands of the original one. Just as Raighby said "grid refinements can reduce these problems, the required degree of refinement is often impracticable for engineering purposes" [63].

The maximum values of the false diffusion in the x, y and z directions and the artificial viscosity in a vertical section are near the burner region as shown in Fig. 12(b), while the maximum turbulent viscosity is located in the center of the vertical section. The large false diffusion affected zone needs special care for the mesh design and the convective treatment in the TFF flow simulations.

7. Comparison of rectangular and body-fitted mesh predictions of combustion processes

7.1 Modeling object and mesh topology

A structured rectangular mesh and a structured body-fitted mesh both with the first-order upwind scheme were used to simulate the comprehensive combustion processes in a tangentially fired utility boiler (HG-670/140-9 boiler with a steam production of 670t/h) which is twenty times the size of the scale furnace model in Fig. 6. The air velocity, temperature and species distributions predicted by using these two meshes were compared to evaluate the numerical diffusion effects in the comprehensive TFF combustion simulation. The body-fitted and the rectangular meshes in the TFF comprehensive combustion simulations are shown in Fig. 13.

To simplify the model, the furnace hopper was modeled as a cube in the numerical simulations.

7.2 Combustion models

The simulations of combustion in the TFF used the following models:

7.2.1 Coal particle trajectory model

The Lagrangian method was used to simulate the particle trajectories. A particle force analysis indicated that [64] gravity, pressure differences across the particles, the magnus force and the Basset force could be neglected. The particle momentum equation is then:

$$m_p \frac{dV_{pi}}{dt} = \frac{1}{2} C_D \rho A_p \left(V_f - V_{Pi}\right)\left|V_f - V_p\right| + m_p g_i \quad (21)$$

where mp is the particle mass.

The non-spherical effects and the Stephen flux effects on the combustion were included [65, 66] by calculation C_D as:

$$C_D = C_{sp}\left(1 + 0.862 \lg \varphi\right)^{-1} \frac{B_k}{\exp\left(B_k\right) - 1} \quad (22)$$

7.2.2 Devolatilization model

The pyrolysis was modeled using Stickler's parallel Eqs. (25-27) [67] for the reaction rate:

$$\dot{m}_{c,1} = m_c \alpha_1 k_1 \exp(-E_1 / RT) \quad (23)$$

$$\dot{m}_{c,2} = m_c \alpha_2 k_2 \exp(-E_2 / RT) \quad (24)$$

$$\dot{m}_v = \dot{m}_{c,1} + \dot{m}_{c,2} \quad (25)$$

7.2.3 Heterogeneous char reaction model

The char combustion models used a diffusion-controlled model including pore effects on the internal surface of the char. The char combustion was simplified into two reactions with the diameters and densities of the char particles varying during the devolatilization.

$$\begin{aligned} C + \frac{1}{2} O_2 &\rightarrow CO \\ CO + \frac{1}{2} O_2 &\rightarrow CO_2 \end{aligned} \quad (26)$$

7.2.4 Gas-phase combustion model

The volatiles combustion is the main part of the gas-phase reaction besides the carbon monoxide oxidation. The EBU model proposed by Spalding was used to simulate the gas-phase turbulent reaction [68]. The release, combustion, and diffusion of O_2, CO_2, CO, H_2O, and C_nH_m were expressed mathematically as the following general convection-diffusion equation in curvilinear coordinates:

$$C_n H_m + \left(n + \frac{m}{4}\right) O_2 \rightarrow n CO_2 + \frac{m}{2} H_2 O \quad (27)$$

$$\begin{aligned} &\frac{\partial}{\partial \xi^j}\left(\frac{\rho V^j}{J} \cdot f_s\right) = \frac{\partial}{\partial \xi^j}\left(\frac{\mu}{\sigma_s} \frac{g^i g^k}{J} \frac{\partial f_s}{\partial \xi^i}\right) \\ &+ \left(S_{ps} + \min\left(\bar{w}_{s,T}, \bar{w}_{s,A}\right)\right) \frac{1}{J} \end{aligned} \quad (28)$$

where,

S_{ps} gas generation source
$\bar{w}_{s,T}$ turbulent diffusion-limited reaction rate
$\bar{w}_{s,A}$ kinetics-limited reaction rate of Arrhenius approximation

The particle Lagrangian energy equation with heterogeneous heat transfer between the gas and solid phases was:

$$\begin{aligned} &m_p C_p \frac{dT_p}{dt} = \pi d_k \lambda Nu_k \frac{B_k}{\exp\left(B_k\right) - 1}\left(T_g - T_p\right) \\ &+ Q_h + Q_w + \kappa_p \left(\int_{\Omega:0 \rightarrow 4\pi} I d\Omega - 4\sigma^B T_p^4\right) \end{aligned} \quad (29)$$

where,

Q_h Heat release from char
Q_w Vapor latent heat
The gas-phase energy equation was:

$$\frac{\partial}{\partial \xi^i}\left(\frac{\rho u^i}{J}\cdot h_g\right)=\frac{\partial}{\partial \xi^i}\left(\frac{\lambda_T}{C_g}\frac{\vec{g}^i\cdot\vec{g}^k}{J}\frac{\partial h_g}{\partial \xi^j}\right) +\left(q_p+w_f Q_f+\kappa_g\left(\int_{\Omega:0\to 4\pi} Id\Omega-4\sigma^B T_g^4\right)\right)\frac{1}{J} \tag{30}$$

where,
q_p Gas-solid convection source
The wall temperature was calculated from the heat transfer from the water inside the water wall and to the flue gas outside the water wall.

$$T^w=\varepsilon^w\left(q_c^w+q_r^w\right)+T^a \tag{31}$$

where,
ε_w Overall thermal resistance from the wall to the flue gas
q_{cw} Convection heat flux from gas to wall
q_{rw} Radiation heat flux from gas to wall
T_a Water temperature in screen wall
The mean physical properties of the gas were based on the gas properties and concentrations. The calculation of these properties is described in detail by Robert et al. [69].

Radiation Model

The radiation transfer equation (RTE) was used to simulate the thermal radiation. Viskanta and Menguc [34] reviewed radiative process simulation models used for combustion and discussed the RTE solution and the radiative properties of the flue gas and the particles in detail.

$$\left(\bar{\Omega}\cdot\nabla\right)I\left(\bar{r},\bar{\Omega}\right)=-\left(\alpha+\sigma\right)I\left(\bar{r},\bar{\Omega}\right)+ \kappa I_b\left(\bar{r}\right)+\frac{\sigma}{4\pi}\int_{\Omega'=4\pi} I\left(\bar{r},\bar{\Omega}'\right)\Phi\left(\bar{\Omega}'\to\bar{\Omega}\right)d\bar{\Omega}'$$

where,
α Absorption coefficient
σ Scattering coefficient
The discrete ordinates (DO) method was used to solve the algebraic radiation equations because of its efficiency and accuracy. The most important reason for selecting the DO model to model the radiation heat transfer in the TFF was its effective adaptability to both in Cartesian and curvilinear mesh systems.

7.3 Simulation results comparison

Inaccurate flow field predictions will affect the other scalar convection-diffusion processes so that combustion simulations will be inaccurate. Therefore, fluid dynamics simulations with less false diffusion will provide better simulations of the combustion processes in the TFF.

The simulated velocity fields in the TFF at a height of 1600 cm in the utility boiler HG-670/140-9 predicted using the body-fitted and rectangular meshes are compared in Fig. 1. The injected flow in the rectangular mesh is quickly attenuated because of the strong crossflow diffusion effects introduced by the first order upwind scheme so that the injected flows from the burner incorrectly reach the water wall very quickly. In the body-fitted mesh, the injected flows reach further out into the center of the furnace to form a swirling counter-clockwise rotation. Comparison of the temperature distributions at a height of 1600 cm in Fig. 14 shows that a more accurate predicted injection flow in the body-fitted mesh resulted in very different temperature distributions with lower temperatures along the wall in the rectangular mesh results and a larger hot section in the middle as the injection flows were quickly deflected towards the wall. The gas species distributions in the two meshes were also quite different due to the different predicted injection structures. For instance, the flue gas production and the heat release predicted by using the body-fitted mesh were concentrated in the narrow region near the injectors with a high temperature region downstream of the injections. In the rectangular mesh, the heat sources were more dispersed inside the furnace so the high temperature area was larger as shown in Fig. 14.

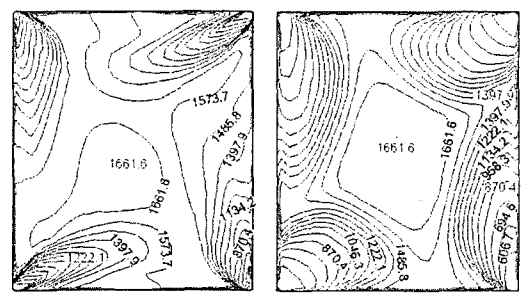

(a) Body-fit mesh (b) Rectangular mesh

Fig. 14. Temperature contour comparison in cross-section plane.

The velocity distribution in the rectangular mesh resulted in the particles and combustible species being completely burned out near the injectors, while in the body-fitted mesh, the relatively higher velocities resulted in entrained particles and the combustible species burning over a longer distance. Thus, the temperatures above the burners in the body-fitted mesh results were higher than the temperatures above the burners in the rectangular mesh results as shown in Fig. 15.

The gas-solid radiation heat transfer is also strongly affected by the temperature distribution. Most of the reaction rates are temperature dependent so the temperatures also affect the particle trajectories and the slagging on the water walls. The different temperature contours shown in Fig. 15 resulted in very different particle dispersion results.

The O_2 concentrations also differed greatly in the two numerical simulations as shown in Fig. 16 because cause of the different predicted injection structures in the two meshes. The O_2 concentrations decreased quickly normal to the streamwise direction in the body-fitted mesh with a relatively low O_2 concentration in the furnace. However, the opposite phenomenon was observed in the rectangular mesh results with the O_2 concentration decreasing more along the streamwise direction.

Experimental validation is the further work to be continued.

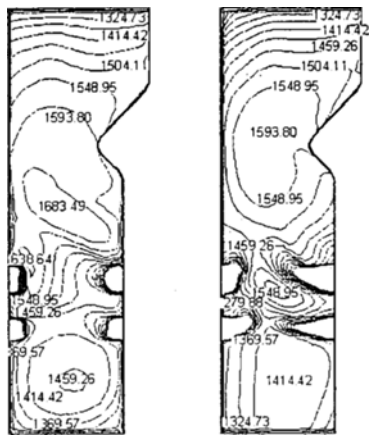

(a) Body-fitted mesh (b) Rectangular mesh

Fig. 15. Combustion temperature contours in the vertical plane

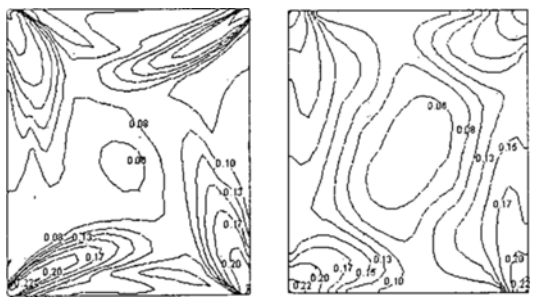

(a) Body-fitted mesh (b) Rectangular-mesh

Fig. 16. O_2 concentration at a height of 1600 cm

8. Conclusions

Higher-order convective schemes must be used to obtain accurate combustion simulations along with better mesh designs for engineering applications. In coal combustion modeling in the TFF, the body-fitted mesh arrangement and higher-order upwind advection schemes significantly reduced the numerical false diffusion near the four corners. Many computational examples have shown that the fluid dynamics computation in the TFF can play a critical role in the comprehensive TFF simulation. Inaccurate flow field predictions make the other scalar convection-diffusion results less meaningful.

Qualitative observations and quantitative validations have shown that the simple rectangular mesh combined with the first-order upwind scheme leads to severe false diffusion. The refined rectangular mesh reduces the numerical diffusion only if the refined elements are sufficiently small. Higher-order upwind schemes in the rectangular mesh are helpful to reduce this numerical error. The mesh investigation showed that grid line adjustments (the O type mesh or the body-fitted mesh) more effectively reduce false diffusion than simply refining the rectangular mesh. When the O type mesh is employed in the TFF combustion simulation, the size of the central small rectangle used to generate the grid lines in the furnace center should be carefully selected since smaller rectangles will result in less false diffusion in the central region. If the central rectangle is the same size as the furnace, the O type mesh will be a rectangular mesh with serious numerical diffusion.

Analysis of the crossflow diffusion in the TFF showed that near the injection nozzles, the x-, y- and z-direction crossflow diffusions coefficients were much higher than elsewhere inside the furnace with the false diffusion being 10-30 times higher in these regions than the turbulent viscosity. These diffusion effects imply that the x-direction diffusion effect can

be reduced to the same level as the actual physical diffusion in the convection-diffusion equation if the grid size in each direction in the rectangular mesh is reduced to one-tenth of the original size resulting in 1000 times as many cells, which is a considerable computational expense.

The flue gas velocities predicted by using the two meshes also remarkably affected the other scalar distributions and the particle behavior inside the TFF. Predictions with different mesh topologies resulted in significantly different distributions of some important physical variables such as the temperature and species concentrations, even though the comprehensive combustion models were the same. Therefore, the accurate comprehensive combustion modeling in a TFF will not be correct if significant false diffusion is present.

Fig. 2 shows that the mesh adjustments of the grid lines to reduce the cross diffusion may increase the streamwise diffusion effect when the first-order upwind scheme is used, but the product of the streamwise diffusion coefficient and $\partial^2\phi/\partial s^2$ is normally negligible compared to the crossflow diffusion effect since $\partial^2\phi/\partial s^2$ is very small.

Nomenclature

ρ	: Fluid density
|V|	: Velocity magnitude
u, v, w	: Velocity components in x, y, z directions
θ	: Angle between the velocity and the x-axis
ϕ	: Scalar (velocity components, kinetic energy, enthalpy, etc.)
$\tilde{\phi}$	: Normalized scalar
Γ	: Coefficients of diffusion term in convection-diffusion equation
$\Gamma'_s, \Gamma'_n, \Gamma'_{sn}$	: False diffusion coefficients in multi-dimensional approximation
$\Gamma_{cfx}\Gamma_{cfy},\Gamma_{cfz}$	: False diffusion coefficients in x, y, z directions
Δx, Δy,Δz	: Grid interval in x, y, z directions
p_k	: Exponential function
$\boldsymbol{J}$	: Jacobian transformation matrix
V_i	: Contravariant velocity in curvilinear coordinate system
k	: Turbulent energy
ε	: Turbulent energy dissipation rate
μ	: Dynamic viscosity
ν	: Kinematic viscosity
T	: Temperature
k_1, k_2	: Kinetic parameters in parallel pyrolysis process equations
E_1, E_2	: Activation energies in parallel pyrolysis process equations
C_D	: Drag force coefficient
$\bar{w}_{s,T}$	: Turbulent diffusion-limited reaction rate
$\bar{w}_{s,A}$	: Kinetics-limited reaction rate in Arrhenius approximation
Q_h	: Heat release from char
Q_w	: Vapor latent heat
q_{cw}	: Convection heat flux from gas to wall
q_{rw}	: Radiation heat flux from gas to wall
T_a	: Water temperature in the water wall
α	: Absorption coefficient
σ	: Scattering coefficient

References

[1] R. W. Bilger. Future progress in turbulent combustion research, *Prog Energy Combust Sci.* (2000) 367-380.

[2] W. Pan, Z. H. Chi, D. B. Si, T. Ruan and K. F. Cen, Numerical simulation of combustion process in a 200MW tangentially fired furnace to study furnace reconstruction, *Proceedings of the CSEE.* 25 (8) (2005) 80-84.

[3] C. G. Yin, L. Ronsendahl and T. J. Cordra, Further study of the gas temperature deviation in large-scale tangentially coal-fired boilers, *Fuel.* 82 (2003) 1127-1137.

[4] X. J. Liu, X. C. Xu and H. L. Fan, Further studies on the coal combustion behavior in the tangentially fired boiler furnace, *Proceedings of the CSEE.* 21 (1) (2001) 81-84.

[5] B. P. Leonard and J. E. Drummon, Why you should not use 'Hybrid', 'Power-low' or related exponential schemes for connective modeling-There are much better alternatives, *Int. J. Numer. Methods Fluids.* 20 (1995) 421-442.

[6] B. P. Leonard, Bounded high-order upwind multidimensional finite-volume convection-diffusion algorithm, In- Minkowycz W J, Sparrow E M, eds. *Advances in numerical heat transfer.* Vol. 1; New York- Taylor & Francis 20 (5) (1997) 23-25.

[7] P. J. Roach, Computational fluid dynamics, Hermosa, Albuquerque, NM, (1972).

[8] G. D. Raighby, A Critical evaluation of upstream differencing applied to problems involving fluid flow, *Com. Meth. Appl. Mech. Eng.* 9 (1976) 75-103.

[9] C. A. J. Fletcher, In: Peyret R, Taylor TD, editors. Computational techniques for fluid dynamic, volume I - fundamental and general techniques, 2nd ed. Berlin: Springer-Verlag. (1991) 327.

[10] Y. H. Kang, W. G. Michael and P. M. Vincent, A method for reduction of numerical diffusion in the donor cell treatment of convection, *J. Computational Physics.* 63 (1986) 201-221.

[11] B. P. Leonard, Bounded high-order upwind multidimensional finite-volume convection-diffusion algorithm. In- Minkowycz W J, Sparrow E M, eds. Advances in numerical heat transfer, Vol. 1. New York- Taylor & Francis, 20 (5) (1997) 23-25.

[12] M. S. Darwish and F. Moukalled, The normalized weighting factor method- a novel technique accelerating the convergence of high-resolution convergence schemes. *Numer Heat Transfer B.* 30 (1996) 217-237.

[13] S. K. Choi, H. Y. Nam and M. Cho, Evaluation of a higher-order bounded convection scheme- three-dimensional numerical experiment. *Numer Heat Transfer. Part B.* 28 (1995) 23-28.

[14] B. P. Leonard, The EULER-QUICK code. In- Taylor C, Morgan K, eds. Numerical methods in laminar and turbulent flows. Swansea- Pineridge Press, (1983).

[15] J. Zhu, M. A. Leschziner, A local oscillation-damping algorithm for higher-order convection schemes, *Comput. Meth. Appl. Mech. Eng.* 67 (1988) 355-366.

[16] J. Zhu and W. Rodi, A low-dispersion and bounded convection scheme. Comput. Meth. Appl. Mech. Eng. 92 (1991) 87-96.

[17] B. Van Leer, Towards the ultimate conservation difference scheme V. A second-order sequel to Godunov method, *J. Comput. Phys.* 23 (1977) 101-136.

[18] S. R. Chakravarthy and S. Osher, High resolution applications of the OSHER upwind scheme for the Euler equations. AIAA paper 1943; 1983.

[19] G. D. Raithby, Skew upwind Differencing Schemes for Problems Involving Fluid Flow, *Comput. Meths. Appl. Mech. Eng.* 9 (1976) 153-164.

[20] X. Y. Zhou, C. G. Zheng, Comparison of several discrete arithmetic schemes for simulating a constrained jet and a lab-scale tangential fired furnace. *Computer Methods in Applied Mechanics and Engineering.*130 (1996) 279-288.

[21] Z. G. Wang, Y. Q. Zhuo, C. H. Chen et al, Mesh Investigation about Crossflow Diffusion of Computational Flow Dynamics in Tangential Combustion Flow Field. *Proceedings of the CSEE.* 27 (5) (2007) 22-28.

[22] J. F. Thompson, Z. Warsi and C. W. Mastin, Numerical Mesh Generation. New York: Elsevier, (1982).

[23] J. F. Thompson, Z. Warsi and C. W. Mastin, Numerical Mesh Generation. New York: Elsevier, (1982).

[24] S. A. Niksa, Coal combustin modeling, IEA coal research Report IEAPER/31, (1996).

[25] B. Jamal and M. F. Mereb, Abbott CONSOL Inc. Research and Development, Comparing pulverized coal reburning in wall and tangential firing configurations.

[26] Z. Chen, Proceedings of the International Technical Conference on Coal Utilization & Fuel Systems 1 (27) (2002) 549-560.

[27] B. S. Brewster, S. C. Hill, P. T. Radulovic and L. D. Smoot, In: Smoot LD, editor. Fundamentals of coal combustion for clean and efficient use. Amsterdam: Elsevier, (1993).

[28] A. M. Eaton, L. D. Smoot, S. C. Hill and C. N. Eatough, Components, formulations, solutions, evaluation, and application of comprehensive combustion models, *Prog. Energy Combust Sci.* 25 (1999) 387-436.

[29] S. C. Hill and L. D. Smoot, A comprehensive three-dimensional model for simulation of combustion systems- PCGC-3, *Energy & Fuels.* 7 (1993) 874-883.

[30] L. D. Smoot, Modeling of coal-combustion process, *Prog. Energy Combust. Sci.* 10 (1989) 229-272.

[31] C. N. Eastwick, S. J. Pickering and A. Aroussi, Comparisons of two commercial computational fluid dynamics codes in modeling pulverized coal combustion, *Applied Mathematical Modeling.* 23 (1999) 437-446.

[32] C. G. Yin, S. Caillat and J. L. Harion, Investigation of the flow, combustion, heat-transfer and emissions from a 609MW utility tangentially fired pulverized-coal boiler, *Fuel.* 81 (2002) 997-1006.

[33] B. S. He, L. Y. Zhu and J. M. Wang, Computational fluid dynamics based retrofits to reheater

panel overheating of No.3 boiler of Datang Power Plant, *Computer & Fluids*. 36 (2007) 435-444.

[34] R. Viskanta and M. P. Mengut, Radiation heat transfer in combustion systems, *Prog. Energy Combust Sci.* (1987) 97-160.

[35] H. F. Wang and J. N. Harb, Modeling of ash deposition in large-scale combustion facilities burning pulverized coal, *Prog. Energy Combust Sci.* 23 (1997) 267-282.

[36] D. L. Black, M. Q. McQUAY, Particle characteristics in the radiant section of a coal-fired utility boiler, *Combust. Sci. and Tech.* 132 (1998) 37-74.

[37] M. P. Bonin, Queiroz, Local particle velocity, size and concentration measurement in an industrial-scale pulverized coal-fired boiler, *Combustion and Flames*. 85 (1991) 121-133.

[38] D. R. Tree, B. W. Webb, Local temperature measurements in a full-scale utility boiler with overfire air, *Fuel*. 76 (11) (1997) 1057-1066.

[39] F. C. Lockwood, C. Papadonoulos and A. S. Abbs, Prediction of corner-fired power station combustion, *Combust. Sci. Techno.* 58 (1988) 5-23.

[40] V. I. Kouprianov, Modeling the effects of operating conditions on fuel and environmental costs for 310MW boiler firing fuel oil. *Energy Conversion and Management*. 45 (2004) 1-4.

[41] Z. H. Chi, L. H. Shen, J. J. Xia, H. Zhou and X. Jiang, Test and Numerical Simulation of Multiphase Dynamics in Utility Boiler with Concentric Firing System, *Journal Of Combustion Science And Technology*. 3 (2) (1997) 206-214.

[42] J. R. Fan, X. D. Zha, P. Sun and K. F. Cen, Simulation of ash deposit in a pulverized coal-fired boiler. *Fuel*. 80 (2000) 645-654.

[43] J. R. Fan and A. L. Ren, Study on pseudo-diffusion of the numerical simulation of cold flow in tangentially fired furnace, in- Proceedings of the Second International Symposium on Coal Combustion, Peking, (1991) 224-229.

[44] X. J. Liu and X. C. Xu, Comparison of the Influence of Pseudo Diffusion on the Numerical Simulation of Flow Field in a Tangential-Firing Furnace with Different Mesh Systems, *J. Combustion Science Technology*. 3 (2) (1997) 113-119.

[45] C. F. You, H. Y. Qi and X. C. Xu, Numerical simulation of flow field in tangentially fired boiler using different turbulence models and discretization schemes, *Power Engineering*. 21 (1) (2001) 1128-1131.

[46] M. H. Xu, J. W. Yuan, S. F. Ding and H. D. Cao, Simulation of the gas temperature deviation in large-scale tangential coal fired utility boilers. *Comput. Mehtods Appl. Mech. Engrg.* 155 (1998) 369-380.

[47] C. G. Zheng, C. H. Liu, X. N. Duan and B. Y. Gong, A numerical investigation on the performance of a 300MW pulverized coal furnace. *Proceedings of the CSEE*. 20 (6) (2000) 79-83.

[48] J. Xiang, Y. H. Xiong, C. G. Zheng, X. X. Sun, Using PDF -Arrehenius to simulate 3-dimensionally NOx Formation during coal combustion, *Proceedings of the CSEE*. 22 (6) (2002) 156-160.

[49] C. G. Zheng, Z. H. Liu, X. L. Duan and J. C. Mi, Numerical and experimental investigations on the performance of a 300 MW pulverized coal furnace, *Proc combust Inst.* 29 (2002) 811-818.

[50] R. Sun, Y. Wu and J. Swithenbank, Horizontal split combustion burner in a 200MW tangential fired boiler, *Journal of the Energy Institute*. 77 (2004) 97-107.

[51] X. J. Liu and X. C. Xu, Numerical simulation of the flow field in the tangential-firing boiler furnace by using the ale algorithm *Proceedings of the CSEE*. 19 (2) (1999) 1-4.

[52] Z. Zhang, S. H. Wu, Y. K. Qin and X. C. Xu, Close to streamline numerical simulation on complicated structural nozzle jets in furnace flow field, *Proceedings of the CSEE*. 21 (8) (2001) 108-113.

[53] C. H. Zheng, Q. Tang , X. C. Xu, Y. Li, Numerical modeling of 3-D iso-thermal flow in tangentially-fired boiler with body-fitted meshes, *Proceedings. Of CSEE*. 22 (7) (2002) 29-34.

[54] C. H. Zheng and X. C. Xu, Analysis of the effect of stokes number and initial condition on the dispersion character for the solid particles in boiler furnace, *Proceedings of the CSEE*, 23 (1) (2003) 171-176.

[55] L. Li and L. X. Zhou, Simulation of 3-D gas-particle flows and coal combustion in a tangential-fired furnace model using a two-fluid-trajectory model, ACTA AERODYNAMICA SINICA,19 (1) (2001) 30-38.

[56] A. L. Ren and Y. R. Fan, Numerical simulation and experiment study in the complex circular flow field, ACTA AERO -DYNAMICS SNICA, 12 (2) (1994) 178-185.

[57] J. R. Fan, P. Sun, X. D. Zha and K. F. Cen, Modeling of combustion process in 600MW utility boiler using comprehensive models and its experimental validation, *Energy & Fuels*. 13 (1999) 1051-

1057.

[58] J. R. Fan, L. G. Qian, Y. L. Ma and K. F. Cen, Computational modeling of pulverized coal combustion processes in tangentially fired furnaces. *Chemical Engineering Journal.* 81 (2001) 261-269.

[59] Dantec Measurement Tech., PDA Installation and User's Guid, (1994).

[60] C. H. Zheng, Comprehensive Modeling of Coal Combustion in Furnace with Non-orthogonal Body-fitted Meshes. Ph. D. Thesis, (2002).

[61] H. Q. Yang, S. D. Habchi, A. J. Przekwas, General strong conservation formulation of Navier-Stokes equations in nonorthogonal curvilinear coordinates, *AIAA J.* 32 (5) (1994) 936-941.

[62] Z. Q. Tian, Experimental investigation of count flow in tangential firing furnace. *Technique communication.*1 (1972) 1-6.

[63] G. D. Raighby and K. E. Torrance, Upstream-weighted schemes and their application to elliptic problems involving fluid flow, *Computers and Fluids.* 2 (1974) 75-103.

[64] X. G. Shi, X. C. Xu, J. K. Feng, The analysis of forces on particles moving in turbulent flow, *J. Engg. Thermophysics.* 10 (3) (1989) 320-325.

[65] K. F. Cen and J. R. Fan, Combustion Hydrodynamics.Beijing: China Irrigation Works and Electricity Press, (1991).

[66] L. X. Zhou, Numerical simulation for turbulent two-phase flow and combustion. Beijing: *Tsinghua University Press,* (1991).

[67] L. D. Smoot and P. J. Smith, Coal combustion and gasification. New York: Plenum Press, (1985).

[68] Spolding DB, Mixing and chemical reaction in steady unconfined turbulent flames. Process 13th Symp.(int.) on combustion. Pittsburgh, Pennsylvania, The Combustion Insititute, (1971) 649-657.

[69] C. R. Robert, J. M. Prausnitz, B. E. Poling. The properties of gases and liquids. 4th Ed. New York: McGraw-Hill, (1987).